Arabian Journal for Science and Engineering (2022) 47:281–293
https://doi.org/10.1007/s13369-021-05357-5

RESEARCH ARTICLE-CHEMISTRY

Enhanced Removal of Arsenic from Aqueous Medium by Modified Silica Nanospheres: Kinetic and Thermodynamic Studies

Asaad F. Hassan[1,2] · **Radim Hrdina**[2]

Received: 13 September 2020 / Accepted: 13 January 2021 / Published online: 26 January 2021

Abstract

In this study, silica nanospheres (S) and trizma base-modified silica nanospheres (ST2, ST4, ST6, and ST8) were synthesized for the removal of arsenic from aqueous medium with high efficiency. Characterization of the prepared solid adsorbents was performed with different techniques such as thermogravimetric analysis, scanning electron microscopy, X-ray diffraction patterns, transmission electron microscopy, selected area electron diffraction, fast Fourier transform, nitrogen adsorption, point of zero charge (pH_{PZC}), and Fourier transform infrared. Adsorption of As^{+5} was investigated under different application conditions such as adsorbent dosage, pH, shaking time, temperature, and initial As^{+5} concentration. Maximum adsorption capacity reached 64.5 mg g^{-1} at pH 6, 0.9 g L^{-1} as adsorbent dosage, after 60 min of shaking time, and at 25 °C as the optimum adsorption conditions. Adsorption data of As^{+5} by the prepared nanoadsorbents are best fitted with Langmuir, Temkin, and Dubinin–Radushkevich models. Kinetic studies revealed that the adsorption followed pseudo-second-order and Elovich kinetic models. Thermodynamic studies prove that the adsorption process is endothermic, spontaneous, and chemisorption in nature. The most effective desorption was achieved by nitric acid with 99% desorption efficiency. The prepared silica nanospheres solid adsorbents showed a good reusability with 91% adsorption efficiency after four cycles of adsorption and desorption.

Keywords Nanospheres · Arsenic · Adsorption · Thermodynamic · Desorption

1 Introduction

Water pollution with different heavy metal cations such as As^{+5}, Hg^{+2}, Cu^{+2}, Cr^{+6}, Cd^{+2}, and Pb^{+2} is still a major environmental pollution problem affecting all living organisms. The dangerous toxicity nature of those heavy metal cations is due to its non-biodegradability and accumulation in polluted water [1]. As^{+5} is considered as one of the most known toxic pollutants to the environment. As^{+5} is widespread in air, water, and soil with different forms and at different concentrations. It has been found in drinking water and food [2]. The introduction of As^{+5} into the environment is due to combustion of coal [3], metallurgy, agriculture, mining, electronic, and pharmaceutical industries. As^{+5} may be present in either organic or inorganic forms [4]. Arsenite and arsenate are the inorganic forms for aqueous As^{+5} and As^{+3}, respectively. Organic forms for As^{+5} are dimethyl arsenic acid and monomethyl arsenic acid as methylated forms, while aromatic compounds are roxarsone and p-arsanilic acid [5].

According to the World Health Organization (WHO) and US Environmental Protection Agency (US-EPA), the maximum allowed As^{+5} concentration in drinking water is 10 μg L^{-1}[6]. Drinking water polluted with As^{+5} for a long term leads to neurological disorders, hypertension, liver, lung, kidney, bladder cancer, and diabetes [7]. Several methods have been investigated for the removal of As^{+5} from water including physicochemical and biological processes. Ion exchange [8], precipitation [9], adsorption [10–12], coagulation [13], and oxidation [14] were used as physicochemical methods for the removal of As^{+5}. The

Supplementary Information The online version contains supplementary material available at https://doi.org/10.1007/s13369-021-05357-5.

✉ Asaad F. Hassan
asmz68@sci.dmu.edu.eg

1 Department of Chemistry, Faculty of Science, University of Damanhour, Damanhour, Egypt

2 Faculty of Chemical Technology, Institute of Organic Chemistry and Technology, University of Pardubice, Pardubice, Czech Republic

phytoremediation technique is an example of the biological treatment process [15]. Adsorption technique is still the most efficient method in water treatment based on its higher efficiency, low coast, and the easy of solid adsorbent recovery [16]. Solid adsorbents useful in the removal of pollutants must be characterized by higher surface area, higher porosity, modifiable, lower swelling, chemically and thermally stable, water-insoluble, and recoverable. Silicon structure such as silica gel, mesoporous silica (MCM-41), silica nanospheres, and their modified forms is one of the most important solid adsorbents and still used in the field of pollutants adsorption and water treatment. Silica nanospheres were used in many application fields such as wound healing [17], drug delivery [18], catalysis [19], corrosion inhibition [20], analytical application [21], and adsorption [22].

The present work discusses the synthesis of highly porous silica nanospheres using sol–gel method and functionalization with different percentages of 2-amino-2-(hydroxymethyl) propane-1,3-diol (trizma base). Trizma base was selected for silica nanospheres modification because it is characterized by highly water soluble, higher boiling point, and four polar active groups that enhance the adsorption of metal cations. The produced solid adsorbents were characterized by different physiochemical techniques. Batch (static) adsorption of As^{+5} was studied under different adsorption conditions considering the effect of adsorbent dosage, pH of adsorption solution, shaking time, initial adsorbate concentration, and adsorption temperature. Kinetic and thermodynamic parameters for the adsorption of As^{+5} are important to understand the nature and mechanism of the adsorption process. As^{+5} desorption and solid adsorbents reusability were considered after four cycles of the adsorption process.

2 Materials and Methods

2.1 Materials

Cetyltrimethylammonium bromide (CTAB) and 2-amino-2-(hydroxymethyl) propane-1,3-diol (trizma base) were purchased from Sigma-Aldrich Co., St. Louis, MO, USA. Tetraethoxysilane (TEOS) and sodium arsenate heptahydrate ($Na_2HAsO_4 \cdot 7H_2O$) were purchased from Alfa Aesar Co., while ammonia solution, ethanol, chloroform, hydrochloric acid, nitric acid, and sodium hydroxide were purchased from El-Nasr for Pharmaceutical and Chemical Industry Co., Egypt. All the chemicals were used without further purification.

2.2 Synthesis of Silica Nanospheres

The sol–gel method was used in the preparation of highly porous silica nanospheres by applying Najafi et al.'s method [23]. CTAB (0.05125 g) was added into 65 mL mixed solution of ammonia (1 mL) and distilled water (64 mL) into a 250-mL beaker with a continuous magnetic stirrer. 1.0 g of TEOS was added dropwise to the above mixture, and the resulted white slurry was kept at 30 °C for 2 h. The reaction mixture was centrifuged and washed several times with a mixed solvent of water and ethanol (25% v/v) to remove any impurities. The resulted solid material was dried at 80 °C for 2 h followed by calcination at 550 °C for 3 h to remove the residual surfactant (CTAB). The produced solid material (S) was stored in a clean dry bottle.

2.3 Surface Modification of Silica Nanospheres with Trizma Base

Five samples of trizma base-modified silica nanospheres were prepared using a different percentage of trizma base to silica nanospheres (2, 4, 6, and 8%) to obtain ST2, ST4, ST6, and ST8, respectively. In a reaction flask, 0.1 g of silica nanospheres was dispersed in 20 mL of chloroform and mixed with the estimated amount of trizma base with constant stirring. The suspension was refluxed for 8 h and cooled to room temperature. The solid adsorbent was washed with water/ethanol washing solution followed by drying at 80 °C for 4 h to obtain ST2, ST4, ST6, and ST8.

2.4 Characterization of the Prepared Solid Adsorbents

Different characterization techniques were used to identify the thermal stability, textural, and chemical nature of the prepared solid adsorbents. Thermogravimetric analysis curves for S, ST2, ST4, ST6, and ST8 were tested by using a thermoanalyzer apparatus (Shimadzu D-50, Japan) under a nitrogen flow rate of 50 mL min^{-1} and 10 °C at a heating rate up to 800 °C. The percentage weight loss during ignition was calculated for all the solid samples by weighing 0.2 g of the solid adsorbent sample in crucible and put it in the muffle for 6 h at 750 °C till constant weight.

Textural characterizations, namely total pore volume (V_T, $cm^3\ g^{-1}$), surface area (S_{BET}, $m^2\ g^{-1}$), and pore diameter (nm), were determined through nitrogen gas adsorption at − 196 °C by using a NOVA2000 gas sorption analyzer (Quantachrome Corporation, USA).

Solid samples' morphological structure was investigated using a JEOL JSM-6510LV model scanning electron microscope. Transmission electron microscopy (TEM) was studied via a JEOL-JEM-2100 (Tokyo, Japan).

X-ray diffraction patterns (XRD) for S and ST6 (as two selected representative samples) were applied using a D8 Advance diffractometer with a Bragg–Brentano θ–θ goniometer (Bruker AXS, Germany) at room temperature. The used generator was operated at 40 kV and 30 mA.

Point of zero charges for S, ST2, ST4, ST6, and ST8 were determined by the preparation of several closed bottles containing 20 mL of 0.01 mol L^{-1} NaCl, and its pH values were adjusted to values between 2 and 12 using diluted NaOH and/or HCl. The bottles were mixed with 0.1 g of solid adsorbents and agitated for 24 h, and the final pH values were measured using a Hanna pH meter, HI-2200 series. pH_{PZC} is the point at which $pH_{final} = pH_{initial}$ for the curve pH_{final} against $pH_{initial}$ [24].

Fourier transform infrared spectroscopy (FTIR) was performed for all the prepared solid adsorbent samples using a Mattson 5000 FTIR spectrometer in the range 400–4000 cm^{-1} to identify the surface chemical functional groups.

2.5 Adsorption of Arsenic Ions

Batch adsorption experiments were carried out on As^{+5} ion solution under different application conditions to obtain the optimum adsorption conditions, maximum adsorption capacities for the solid adsorbents, kinetics, and thermodynamic adsorption parameters.

Arsenic ions adsorption from aqueous solution onto S, ST2, ST4, ST6, and ST8 was studied by shaking 25 mL of As^{+5} solution having a certain concentration with 0.025 g of the solid adsorbent at constant temperature and pH value for 2 h of shaking time. The previous solution was filtered through a Gooch crucible. The residual As^{+5} concentration was determined in filtrate using a 211 Acusys Atomic Absorption Spectrophotometer, Buck Scientific, USA. The average value was calculated by repeating every measurement three times. The adsorption capacity at equilibrium was determined using the following equation:

$$q_e = \frac{C_i - C_e}{m} \times V \quad (1)$$

where C_i and C_e are the initial and equilibrium As^{+5} concentrations, respectively, V is the solution volume (L), and m is the mass of adsorbent (g). Different adsorption conditions were applied to study the effect of adsorbent dosage (0.3–1.5 g L^{-1}), pH (2–10), shaking time (5–100 min), initial adsorbate concentration (10–250 mg L^{-1}), and applied adsorption temperature (20, 30, and 40 °C). The removal percentage ($R\%$) was calculated using Eq. 2.

$$R\% = \frac{C_i - C_e}{C_i} \times 100. \quad (2)$$

2.6 Adsorption Isotherm Models

Many adsorption models were used for studying the adsorption of As^{+5} onto the investigated solid adsorbents such as Langmuir, Freundlich, Temkin, and Dubinin–Radushkevich models.

2.6.1 Langmuir Adsorption Model

Langmuir model based on the presence of identical and a finite number of equivalent localized adsorption sites on the surface of solid adsorbent and the linear Langmuir adsorption [25] model are derived as:

$$\frac{C_e}{q_e} = \frac{1}{bq_m} + \frac{C_e}{q_m} \quad (3)$$

where q_e, q_m, and b are the adsorption capacity at equilibrium (mg g^{-1}), the maximum adsorption capacity (mg g^{-1}), and adsorption constant of Langmuir model (L mg^{-1}), respectively. Calculation of dimensionless separation factor (R_L) gives information on the nature of As^{+5} adsorption, if it is favorable ($0 < R_L < 1$), unfavorable ($R_L > 1$), or irreversible ($R_L = 0$).

$$R_L = \frac{1}{1 + bC_i} \quad (4)$$

where b (L mg^{-1}) and C_i (mg L^{-1}) are Langmuir constant and initial concentrations of As^{+5}, respectively.

2.6.2 Freundlich Adsorption Model

The linear Freundlich model (Eq. 5) was described on the nonideal and reversible nature of the adsorption process [26].

$$\ln q_e = \ln K_F + \left(\frac{1}{n}\right) \ln C_e \quad (5)$$

where n and K_F are the Freundlich constants related to the intensity of adsorption and adsorption capacity, respectively.

2.6.3 Temkin Adsorption Model

The model considers the adsorbate/adsorbent interactions, neglecting the concentration of adsorbate and the linear decrease in heat of adsorption from one layer to the other layer. The model is given by the following equation [27].

$$q_e = ALnK_T + ALnC_e \quad (6)$$

$$A = \frac{RT}{b_T} \tag{7}$$

where the heat of adsorption is related to the constant A, while b_T is the Temkin constant in J mol^{-1}, the gas constant R equals 8.314 J mol^{-1} K^{-1}, T is the Kelvin absolute, and K_T is the Temkin isotherm constant (L g^{-1}).

2.6.4 Dubinin–Radushkevich Adsorption Model

Dubinin–Radushkevich isotherm model differentiates between the adsorption onto homogeneous and heterogeneous surface considering the adsorbate concentration. The linear model is described as follows:

$$\varepsilon = RTLn(1 + \frac{1}{C_e}) \tag{8}$$

$$Lnq_e = Lnq_{DR} - K_{DR}\varepsilon^2 \tag{9}$$

where ε is the Polanyi potential parameter and q_{DR} (mg g^{-1}) and K_{DR} (mol^2 kJ^{-2}) are the maximum adsorption capacity and the activity coefficient, respectively. The gas adsorption constant R equals 8.314 J mol^{-1} K^{-1}, and T is the Kelvin absolute adsorption temperature [28]. Equation 10 is used to calculate the mean adsorption energy ($E_{DR,}$ kJ mol^{-1}):

$$E_{DR} = \frac{1}{\sqrt{2K_{DR}}}. \tag{10}$$

2.7 Adsorption Kinetic Models

Pseudo-first-order (PFO), pseudo-second-order (PSO), and Elovich kinetic models were applied to study the adsorption kinetic parameters of As^{+5} onto the prepared solid samples (Eq. 11, 12, and 13, respectively) [16].

$$\ln(q_e - q_t) = \ln(q_e) - k_1 t \tag{11}$$

$$\frac{t}{q_t} = \frac{1}{k_2 {q_e}^2} + \frac{1}{q_e}t \tag{12}$$

$$q_t = \frac{1}{\beta}\ln \propto \beta + \frac{1}{\beta}\ln t \tag{13}$$

where q_t (mg g^{-1}) is the adsorption capacity measured at certain time. k_1 (min^{-1}) and k_2 (g/mg min^{-1}) are the rate constants of PFO and PSO models, respectively. β represents the extent of surface coverage and the chemisorption activation energy, while α is related to the initial rate of As^{+5} adsorption. The adsorption capacity (q_t) measured at certain time is calculated by the following equation:

$$q_t = \frac{(C_i - C_t)V}{m} \tag{14}$$

where C_t (mg L^{-1}) is the As^{+5} equilibrium concentration at time t.

2.8 Adsorption Thermodynamic Parameters

Equilibrium and thermodynamic adsorption parameters such as the change in entropy ($\Delta S°$), free energy ($\Delta G°$), and enthalpy ($\Delta H°$) are used to investigate the ability, spontaneity, and the heat of As^{+5} adsorption on the investigated solid adsorbents. Equations (15–17) were used in the calculation of equilibrium and thermodynamic adsorption parameters:

$$K_a = \frac{C_s}{C_e} \tag{15}$$

$$LnK_a = \frac{\Delta S^o}{R} - \frac{\Delta H^o}{RT} \tag{16}$$

$$\Delta G^o = \Delta H^o - T\Delta S^o \tag{17}$$

where C_s and C_e (mg L^{-1}) are the surface adsorbed and equilibrium concentrations of As^{+5}, respectively. K_a, R, and T represent the adsorption distribution coefficient, gas constant, and the absolute adsorption temperature, respectively. Plotting Eq. 16 (van't Hoff) enables the calculation of $\Delta H°$ and $\Delta S°$ from the slope and intercept.

2.9 Arsenic Desorption and Solid Adsorbent Reusability

Surface-adsorbed As^{+5} was desorbed by shaking of 0.1 g of ST4 pre-loaded with As^{+5} in 50 mL of distilled water, 1.0 mol L^{-1} nitric acid, or 1.0 mol L^{-1} hydrochloric acid for 2 h. The previous mixture was filtered, and the desorbed As^{+5} was measured in the filtrate. The desorbed quantity was calculated using the following equation [29]:

$$\text{Desorption\%} = \frac{q_i - q_f}{q_i} \times 100 \tag{18}$$

where q_i and q_f are the mass (mg) of As^{+5} on ST4 before and after desorption, respectively.

Solid adsorbent reusability was studied after four cycles of As^{+5}adsorption/desorption process. Adsorption of As^{+5} was carried out by ST4 under the following conditions: 0.025 g L^{-1} as adsorbent dosage, pH 6, 100 mg L^{-1} as As^{+5} initial concentration, 60 min of shaking time, and temperature of 25 °C. After each cycle, the solid adsorbent was filtered and boiled with 30 mL of 1.0 mol L^{-1} nitric acid to desorb the pre-adsorbed As^{+5}, washed with distilled water, and dried at 100 °C for the successive reuse.

3 Results and Discussion

3.1 Characterization of the Synthesized Solid Adsorbents

The % weight loss on ignition at 750 °C was found to be 2.65, 4.71, 6.62, 8.53, and 10.52% for S, ST2, ST4, ST6, and ST8, respectively. The increase in loss in ignition for trizma base-modified samples is due to the total combustion of the organic trizma base compound at higher temperature.

Thermogravimetric curves were used to study the thermal stability of S, ST2, ST4, ST6, and ST8. As presented in Fig. 1a, the weight loss at 110 °C (0.5 and 0.9% for S and trizma base-treated samples, respectively) is due to the evaporation of surface adsorbed water, indicating that trizma base raises the surface hydrophilicity for the treated samples [16]. The slight weight loss observed in the range 200–300 °C may be related to the evaporation of residual occluded water molecules in the internal pores of nanomaterials solid adsorbents. The observable weight loss in the range from 375 to 500 °C which represents about 2.5–4.0% for all the samples may be related to the partial destruction of the template [30]. The observed weight loss at $T > 500$ °C in the case of S sample is probably related to the further condensation in the siloxane matrix with water loss. ST2, ST4, ST6, and ST8 showed another thermal decomposition (3.5, 5.0, 5.2, and 5.4%, respectively) which may be related to the destruction of trizma base. TGA curves prove the thermal stability of the prepared solid samples and its uses at higher application temperatures.

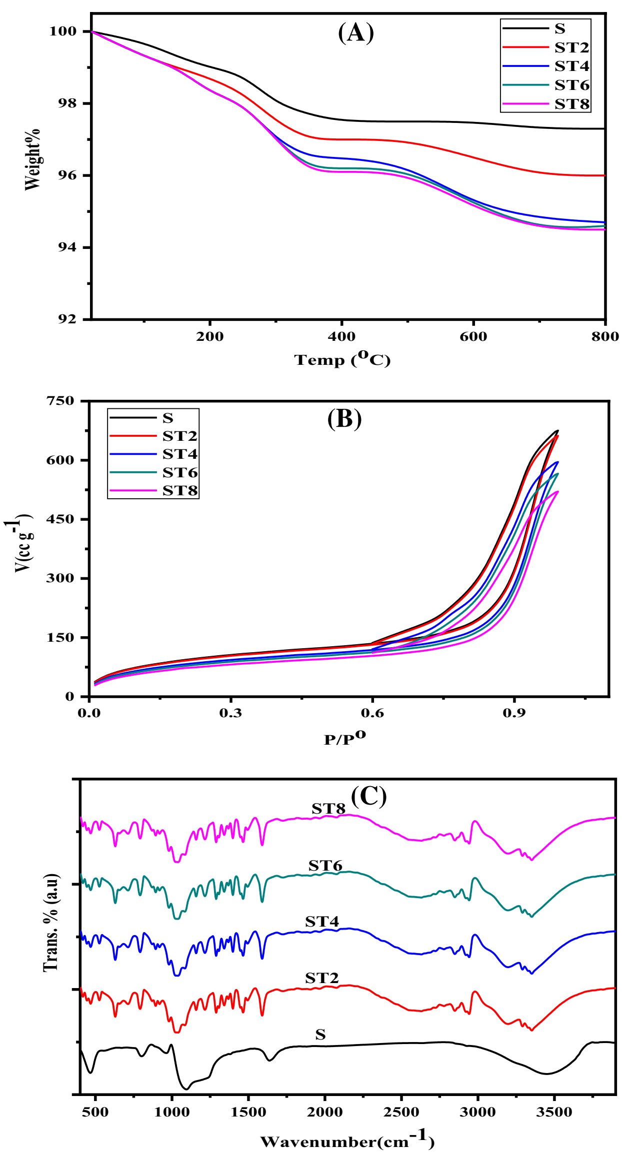

Fig. 1 TGA curves (**a**), nitrogen adsorption/desorption isotherms (**b**), and FTIR spectra (**c**) for S, ST2, ST4, ST6, and ST8

Figure S1A shows the XRD patterns of S and ST6. The XRD patterns confirmed that both of modified and unmodified nanosilica spheres were amorphous SiO_2 based on the broad peak located around $2\theta \approx 22°$ [31–33]

The BET surface area, total pore volume, and pore diameters were calculated for all the samples. Figure 1b shows that all the nitrogen adsorption isotherms followed typical IV adsorption isotherm which belongs to the adsorption onto mesoporous materials where the formation of multilayers at lower pressure and capillary condensation takes place at higher adsorption pressures. The calculated texture pore structures are presented in Table 1. The BET surface area for S was found to be 435.32 $m^2\ g^{-1}$ and slightly decreased for ST2, ST4, ST6, and ST8, which may be related to the blocking of some pores by the effect of trizma base incorporation [23]. Total pore volume ranged between 0.81 and 1.05 $cm^3\ g^{-1}$ which decreases with trizma base modification and proportional with the BET surface area. The pore diameter (8.07–9.68 nm) measurements indicate that the samples are mesopores. All the samples exhibit hysteresis loops of H3 type according to IUPAC classification, and it is related to the slit-like pores originated from the aggregation of nanoparticles [34]. Pore size distribution curves (Fig. S1B) showed that pore diameter for trizma base-modified and unmodified solid samples ranged between 7.12 and 9.03 nm.

Table 1 pH_{PZC} and textural characterization of S, ST2, ST4, ST6, and ST8 derived from nitrogen adsorption isotherms

Textural parameters	S	ST2	ST4	ST6	ST8
S_{BET} ($m^2\ g^{-1}$)	435.32	426.33	417.60	410.51	401.22
V_T ($cm^3\ g^{-1}$)	1.05	1.03	0.92	0.88	0.81
Pore diameter (nm)	9.68	9.65	8.84	8.55	8.07
pH_{PZC}	5.0	5.4	5.4	5.6	5.7

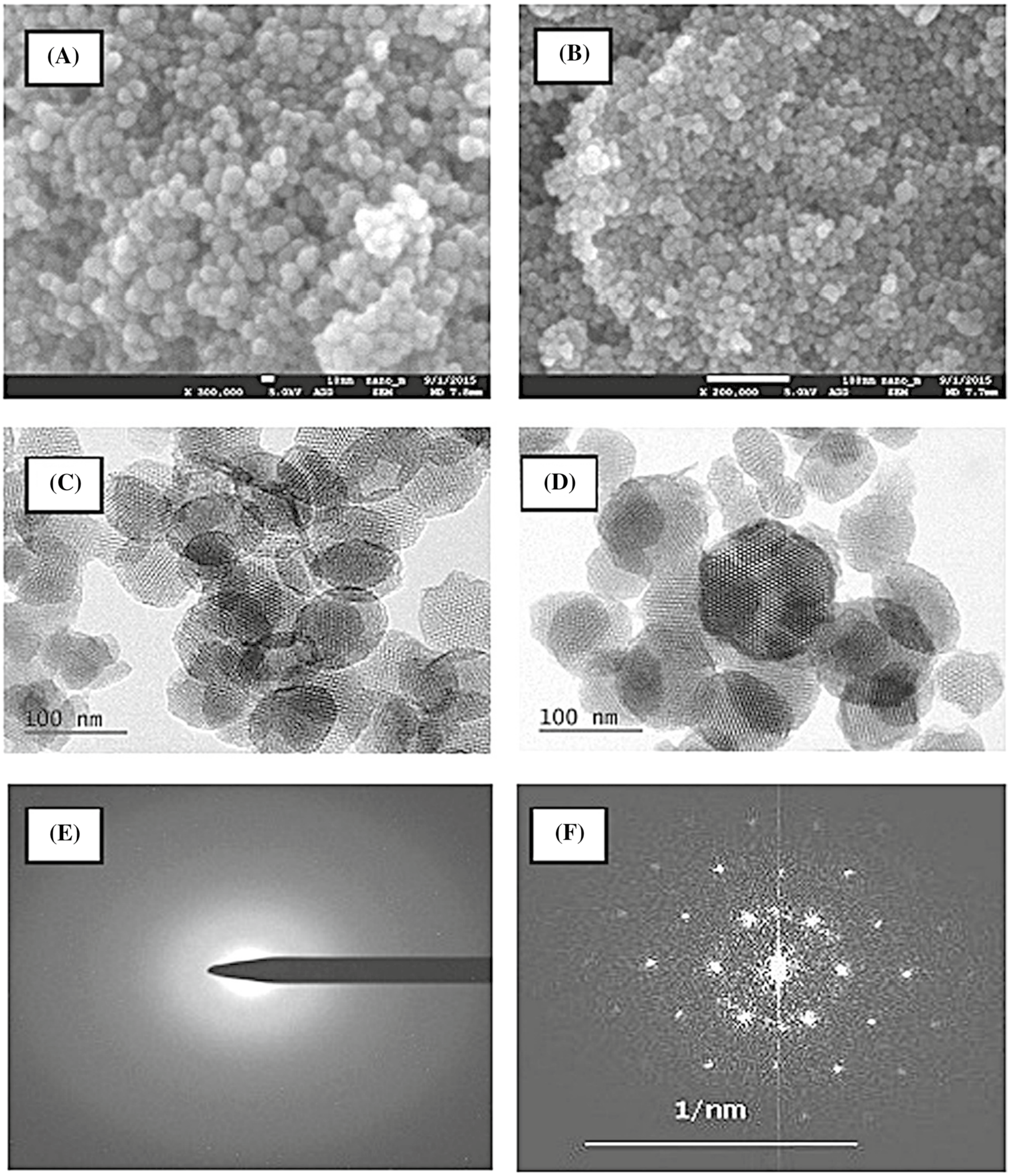

Fig. 2 SEM (**a**, **b**) and TEM (**c**, **d**) images for S and ST4, respectively, SAED (**e**) and FFT (**f**) patterns for S

Surface chemical functional groups on S, ST2, ST4, ST6, and ST8 were examined by means of FTIR spectra. Figure 1c shows that for S sample the broad peak located at 3450 cm^{-1} is due to silanol groups [35], the peaks located at 460 and 967 cm^{-1} are related to bending and stretching vibrations of Si–O-Si groups, respectively [36], and the bands at 805 and 1095 cm^{-1} are corresponding to symmetric and asymmetric stretching vibration modes of Si–O groups [37]. Modified samples with trizma base (ST2, ST4, ST6, and ST8) exhibited the same FTIR peaks where several new bands appeared at 1100, 1550, 2900, and 3386 cm^{-1} indicating the presence of C–C–C, C–N, C–H, and N–H groups, respectively. The overlapping between N–H stretching bands with the broad band of silanol stretching (Si–O–Si) confirms the introduction of NH_2 groups to nanosilica surface [23, 38]. The measured pH_{PZC} values (Table 1) for S, ST2, ST4, ST6, and ST8 were found to be 5.0, 5.4, 5.4, 5.6, and 5.7, respectively.

Two samples were selected for SEM and TEM analysis (S and ST4) and are shown in Fig. 2. Figure 2a, b shows SEM morphologies of the silica nanospheres for S and ST4. SEM images revealed the uniform size of spheres with a smooth surface, in contact, and with a size of nearly 100 nm. Modification of silica nanospheres with trizma base not affects the morphological appearance of spheres, which means that it is only chemical modification [39]. TEM images for S and ST4 samples are displayed in Fig. 2c, d, which clearly revealed that the particles are spherical in shape, with high porosity and with an average particle size of 95 nm. The selected area electron diffraction of S sample (SAED, Fig. 2e) revealed that the prepared solid sample is amorphous in nature. Figure 2f shows a fast Fourier transform (FFT) for S sample, indicating the regular arrangement of pores which confirms the homogenous distribution of pores on the nanosilica surface.

3.2 Adsorption of Arsenic onto all the Prepared Solids

3.2.1 Effect of Nanoadsorbent Dosage

The effect of S, ST2, ST4, ST6, and ST8 dosages on As^{+5} removal was studied, and the obtained results are graphed in Fig. 3a. Figure 3a shows the effect of adsorbent dosage (0.3–1.5 g L^{-1}), while Eq. 2 was used to determine the removal % of As^{+5} from 25 mL of 100 mg L^{-1} as initial concentration at 25 °C, pH 7, and after 120 min of shaking time. It is evident that solid adsorbents dosage with the same behavior where $R\%$ increases with the increase in dosage up to 0.9 g L^{-1}. The previous observation is related to the increase in active sites on the adsorbent surface with the increase in adsorbent mass [40]. There is no observable increase in As^{+5} removal at solid dosage more than 0.9 g L^{-1} which can be related to the adsorption equilibrium establishment at the lower relative As^{+5} concentration compared with the excessive active sites present on the solid adsorbents. The adsorption process of As^{+5} onto all the used solid adsorbents gave an optimum adsorption condition using 0.9 g L^{-1} with a maximum removal percentage of 58, 70, 80, 80, and 85% for S, ST2, ST6, ST8, and ST4, respectively.

3.2.2 Effect of Initial pH

pH value plays an important role in the adsorption capacity and mechanism for metal cations adsorption from aqueous medium onto solid adsorbents. The effect of initial pH of As^{+5} solution was studied in the range 2–10, using 25 mL of 100 mg L^{-1} As^{+5} solution, 0.023 g of sorbent, at 25 °C, and after 120 min of shaking time. The effect of pH is represented in Fig. 3b where the removal efficiency increased when pH values increased from 2.0 to 6.0 for all the samples

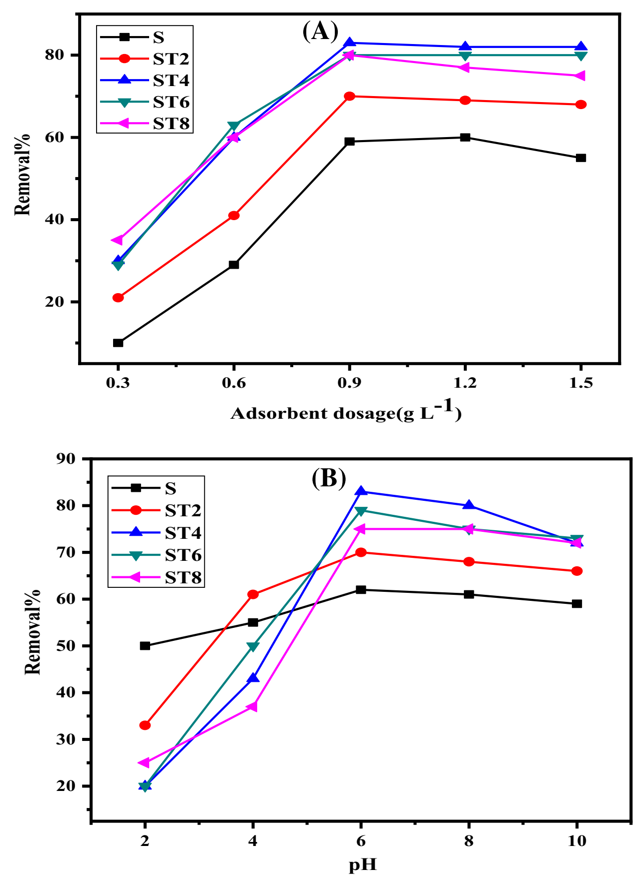

Fig. 3 Effect of initial adsorbent dosage (**a**) and the effect of pH (**b**) on adsorption of As^{+5} onto S, ST2, ST4, ST6, and ST8 at 25 °C

and at pH values more than 6.0 a slight decrease in the removal percentage was observed. The maximum removal capacity was measured at pH around 6.0. This behavior can be explained on the basis of adsorbent surface charges and the speciation of As^{+5} ions. Considering the pH_{PZC} for all the prepared nanosolid adsorbents, the surface of all the samples will acquire positive charges at pH less than its pH_{PZC} and negative at pH higher than its pH_{PZC}. The lower adsorption capacity at lower pH values can be related to the competition between H_3O^+ and As^{+5} on the adsorption sites, and the non-ionic form of As^{+5}, H_3AsO_4 originated at lower pH (at pH < 9.2) will reduce its adsorption process [41]. At higher pH values, the slight decrease in As^{+5} adsorption is due to the electrostatic repulsion between the negatively charged surface of solid adsorbents and the established negative forms of As^{+5} ($H_2AsO_4{}^{-1}$ and/or $HAsO_4{}^{-2}$) [42].

3.2.3 Effect of Contact Shaking Time and Kinetic Parameters

To understand the adsorption rate-limiting step and kinetic adsorption, several models have been used. In the present work, the rate of adsorption has been analyzed by the application of pseudo-first-order (PFO, Eq. 11), pseudo-second-order (PSO, Eq. 12), and Elovich (Eq. 13) kinetic models for the adsorption of As^{+5} onto S and ST4 as two selected representative samples. Figure 4a shows the adsorption capacities of the solid adsorbents against contact shaking time. The rate of As^{+5} adsorption is fast at the beginning time up to nearly 20 and 40 min for S and ST4, respectively, and that rate becomes slower with time passage till the equilibrium adsorption time (60 min). The higher rate at the beginning of adsorption time can be related to the presence of active adsorption sites on the surface of solid adsorbents, and it is known that the adsorption rate is directly proportional to uncovered active sites [24]. Pseudo-first-order, pseudo-second-order, and Elovich linear kinetic models plots are shown in Fig. S2, Fig. 4b, and Fig. 4c, respectively, while the calculated constants are listed in Table 2. As^{+5} adsorption was well fitted by PSO kinetic models with high values of correlation coefficients ($R^2 > 0.9912$), and the calculated adsorption capacity at equilibrium (q_e, mg g^{-1}) for S and ST4 (43.8 and 65.4 mg g^{-1}) is very close to that calculated from the experimental Langmuir adsorption model (q_m, 41.4 and 64.5 mg g^{-1}). The correlation coefficient values calculated for As^{+5} adsorption using PFO models are nearly high, but the difference between q_e and q_m values is very high (31.2 and 27.5% for S and ST4, respectively). The last result proves that As^{+5} adsorption onto the prepared nanomaterials does not follow the PFO kinetic models. The accepted PSO kinetic model confirms that the dominant mechanism of As^{+5} adsorption is the chemisorption process [5]. The calculated rate constants (k_2, g/mg. min^{-1}) for ST4 > S by about 1.3 times indicate the rate of As^{+5} adsorption onto trizma base-treated samples more than that for untreated samples due to the incorporation of new active surface functional groups. Elovich equation is well applied for the adsorption process based on its higher correlation coefficients which

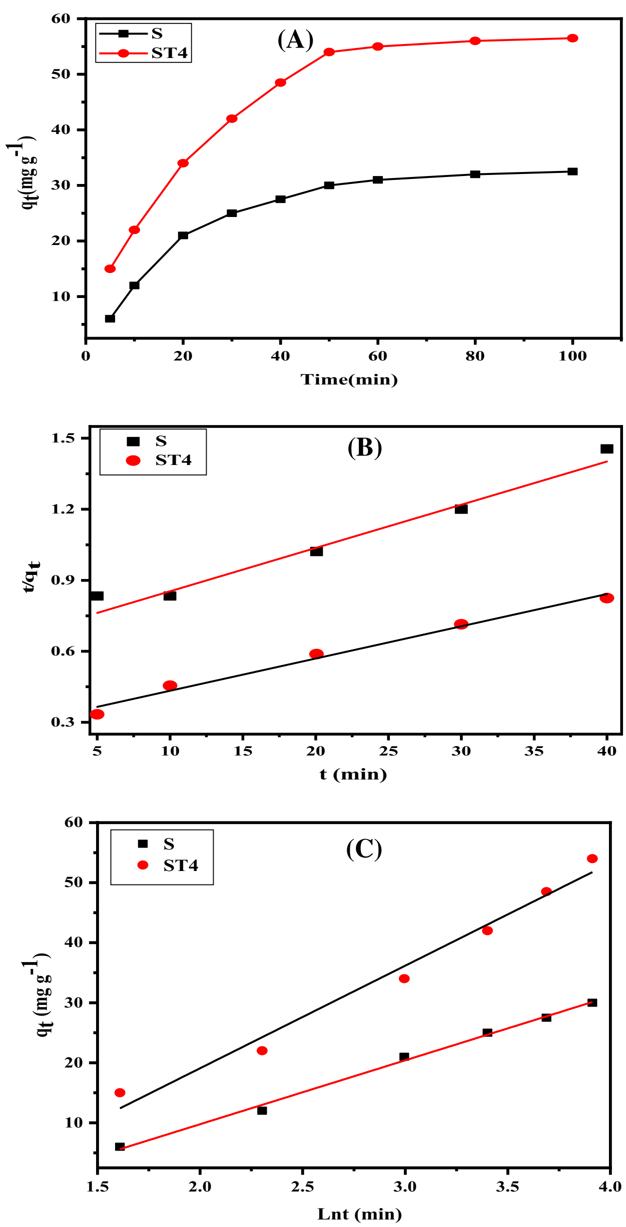

Fig. 4 Effect of contact shaking time (**a**), pseudo-second-order kinetic model (**b**), and Elovich plot (**c**) for the adsorption of As^{+5} onto S and ST4 at 25 °C

Table 2 Pseudo-first-order, pseudo-second order, Elovich kinetic model, and thermodynamic parameters for As^{+5} adsorption onto S and ST4

Parameters	S	ST4
PFO		
q_m (mg g^{-1})	41.4	64.5
q_e (mg g^{-1})	28.5	46.8
k_1 (min^{-1})	0.04803	0.04646
R^2	0.9624	0.9610
PSO		
q_e (mg g^{-1})	43.8	65.4
k_2 (g/mg min^{-1})	4.97×10^{-4}	6.26×10^{-4}
R^2	0.9979	0.9912
Elovich		
α (mg g^{-1} min^{-1})	3.6074	7.0651
β (mg g^{-1})	0.0940	0.0586
R^2	0.9952	0.9756
Thermodynamic parameters		
$\Delta H°$ (kJ mol^{-1})	18.11	12.24
$\Delta S°$ (kJ/mol K^{-1})	0.0713	0.0577
$-\Delta G°$ (kJ mol^{-1})		
20 °C	2.8709	4.6665
30 °C	3.3939	5.2431
40 °C	4.2069	5.8201
R^2	0.9995	0.9671

are 0.9952 and 0.9756 for S and ST4, respectively. The well application of PSO kinetic model indicates that the adsorption of As^{+5} onto trizma-base-treated and untreated silica nanospheres is chemisorption in nature [43].

3.2.4 Effect of Initial Arsenic Ion Concentration

Figure 5a depicts the adsorption isotherms for As^{+5} adsorption onto S, ST2, ST4, ST6, and ST8 at 25 °C considering 0.9 g L^{-1} as the adsorbent dosage, 60-min contact shaking time, pH 6, and 10–250 mg L^{-1} as the initial As^{+5} concentration. The obtained data from the produced adsorption isotherms were analyzed by Eqs. 3, 5, 6, and 9. Figure 5a shows that As^{+5} adsorption is high at a lower initial concentration of As^{+5} ions which may be related to the higher ratio of active adsorbent sites to adsorbate ions and decreased with the increase in that ratio at a higher initial concentration of As^{+5} ions.

Langmuir adsorption model onto the prepared solid samples is predicted in Fig. 5b, while the Langmuir parameter is listed in Table 3. Langmuir model was well applied based on the higher correlation coefficient values (0.9798–0.9968). The calculated maximum adsorption capacity for silica nanospheres was found to be 41.4 mg g^{-1}, while those for ST2, ST4, ST6, and ST8 were 48.2, 64.5, 60.3, and 55.3 mg g^{-1}, respectively, indicating that modification with trizma base raises the adsorption capacity of the modified solid adsorbents which may be related to the addition of new surface functional groups. The maximum adsorption capacity for ST4 was measured to be more than that for S and ST2 by about 55.8 and 33.8%, respectively. As the percentage of trizma base modification increases, the maximum adsorption capacity also increases but till a certain percentage of modifiers which is related to the abundance of surface functional groups present on the main solid material (S). The maximum adsorption capacity for ST4 > ST6 > ST8, can be explained as a result of the decrease in the surface area

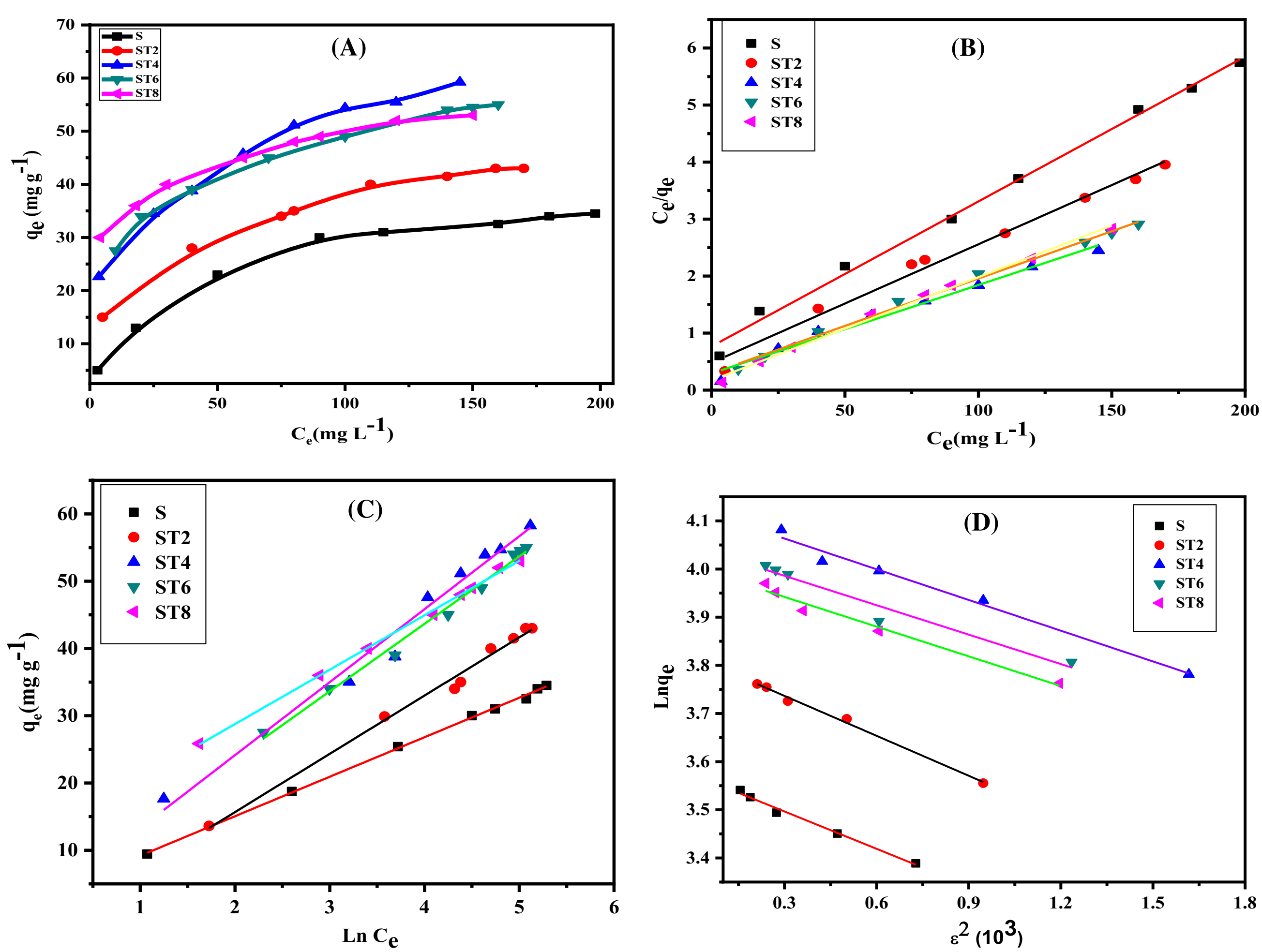

Fig. 5 Adsorption isotherms (**a**), Langmuir (**b**), Temkin (**c**), and Dubinin–Radushkevich (**d**) plots for As^{+5} adsorption onto S, ST2, ST4, ST6, and ST8 at 25 °C

Table 3 Langmuir, Freundlich, Temkin, and Dubinin–Radushkevich adsorption parameters for the adsorption of As^{+2} onto S, ST2, ST4, ST6, and ST8 at 25 °C

Parameters	S	ST2	ST4	ST6	ST8
Langmuir parameters					
q_m (mg g^{-1})	41.4	48.2	64.5	60.3	55.3
b (L mg^{-1})	0.0332	0.0432	0.0529	0.0559	0.1045
R_L	0.3759	0.3165	0.2743	0.2635	0.1606
R^2	0.9944	0.9846	0.9798	0.9939	0.9968
Freundlich parameters					
$1/n$	0.4653	0.3052	0.2648	0.2468	0.1641
K_F	3.27	9.17	15.56	15.81	23.24
R^2	0.8772	0.8672	0.8817	0.7672	0.7876
Temkin parameters					
b_T (J mol^{-1})	443.1	280.2	246.7	246.5	306.0
K_T (L g^{-1})	1.044	1.197	1.969	1.422	1.430
R^2	0.9966	0.9942	0.9711	0.9895	0.9980
Dubinin–Radushkevich parameters					
q_{DR} (mg g^{-1})	39.0	46.0	63.9	58.2	55.1
E_{DR} (kJ mol^{-1})	13.91	13.45	12.33	12.67	12.48
R^2	0.9870	0.9934	0.9792	0.9445	0.9709

without any increase in the surface functional groups. The previous results showed ST4 with the more advanced surface adsorption for As^{+5} from aqueous medium. The calculated R_L values (0.1606–0.3759) confirm the favorable adsorption of As^{+5} onto the prepared solid adsorbents.

Figure S3 shows the Freundlich adsorption equation and the calculated constants in Table 3. The correlation coefficient values (0.7672–0.8817) indicate the poor application of Freundlich models. The well fitting of Langmuir model rather than the Freundlich model indicates the homogeneous monolayer adsorption of As^{+5} on the solid surface [10, 44].

Figure 5c predicts Temkin adsorption model of As^{+5} onto all the prepared nanomaterials, while Temkin constants are illustrated in Table 3. Adsorption data of As^{+5} by the prepared solid silica nanospheres and the modified solids are well fitted by Temkin model as indicated in the higher correlation coefficient values (0.9711–0.9980). The calculated equilibrium binding constants (K_T) for trizma base-modified solid surface (ST2, ST4, ST6, and ST8) are more than that value for unmodified sample (S). The previous observation proves the ability of trizma base to enhance both the adsorption process and the strong binding between modified surface with As^{+5}. The Temkin parameter b_T is related to the heat of As^{+5} adsorption process ($b_T > 80$ J mol^{-1}), which indicates the chemical adsorption of As^{+5} onto the solid surface and the stronger ionic interaction between As^{+5} and the solid surface [45, 46].

The importance of Dubinin–Radushkevich isotherm model (DR) is originated from the consideration of both homogeneous and heterogeneous surface of the solid adsorbents. Figure 5d exhibits the DR for As^{+5} adsorption, and DR parameters are illustrated in Table 3. The adsorption of As^{+5} on the present solids is well fitted with the DR model where R^2 values > 0.9445. The magnitude of maximum adsorption capacity measured by DR model (q_{DR}, mg g^{-1}) is very close to that calculated by the Langmuir model. The magnitude of the mean free energy per ion of As^{+5} during its transformation from solution bulk to the solid adsorbent surface (E_{DR}, kJ mol^{-1}) is in the range 8.0–16.0 kJ mol^{-1} (12.33–13.91 kJ mol^{-1}), indicating that As^{+5} adsorption proceeds via chemisorption or ion exchange mechanism, while values less than 8.0 kJ mol^{-1} represent on physical adsorption [47, 48]. The previous section indicates that As^{+5} adsorption data by S, ST2, ST4, ST6, and ST8 are best fitted with Langmuir, Temkin, and Dubinin–Radushkevich models.

3.2.5 Effect of Adsorption Temperature and Thermodynamic Parameters

Arsenic adsorption was studied onto S and ST4 at 20, 30, and 40 °C under the condition of 0.9 g L^{-1} as adsorbent dosage, pH 6, initial concentration in the range 10–250 mg L^{-1}, and after 60 min of shaking time. Thermodynamic parameters were calculated using Eqs. 15–17. Figure 6a, b and Fig. S4 show the adsorption isotherms, van't Hoff equation (Eq. 16), and applied Langmuir equation at the investigated temperature, respectively. Thermodynamic parameters, namely $\Delta H°$, $\Delta S°$, and $\Delta G°$, are presented in Table 2. Linear fitting of van't Hoff equation was observed from the calculated R^2 values. Upon inspection of thermodynamic parameters, (i) the positive values for entropy changes ($\Delta S°$, 0.0713 and 0.0577 kJ/mol K^{-1} for S and ST4, respectively) reflect the increased As^{+5} randomness during the adsorption process at the solid/liquid interface [49]; (ii) the negative values for free energy change ($\Delta G°$) for As^{+5} adsorption onto untreated and treated solid adsorbents indicate the favorable and spontaneous adsorption process and the increase in the negative values for $\Delta G°$ with temperature reflects the enhanced adsorption at higher temperatures [24]; (iii) the positive values for $\Delta H°$ confirm the endothermic nature for the entire adsorption process; and (iv) the calculated q_m, mg g^{-1} for the solid adsorbents increased with temperature (Table S5) also confirms the endothermic nature for As^{+5} adsorption on the prepared silica nanoparticles.

3.3 Desorption and reusability of adsorbents

Figure 6c illustrates the desorption efficiency of different pure solvent. It indicates that desorption efficiency for $HNO_3 > HCl > H_2O$ (99, 45, and 5%, respectively). Reusability of ST4 was tested for after four cycles of As^{+5} adsorption

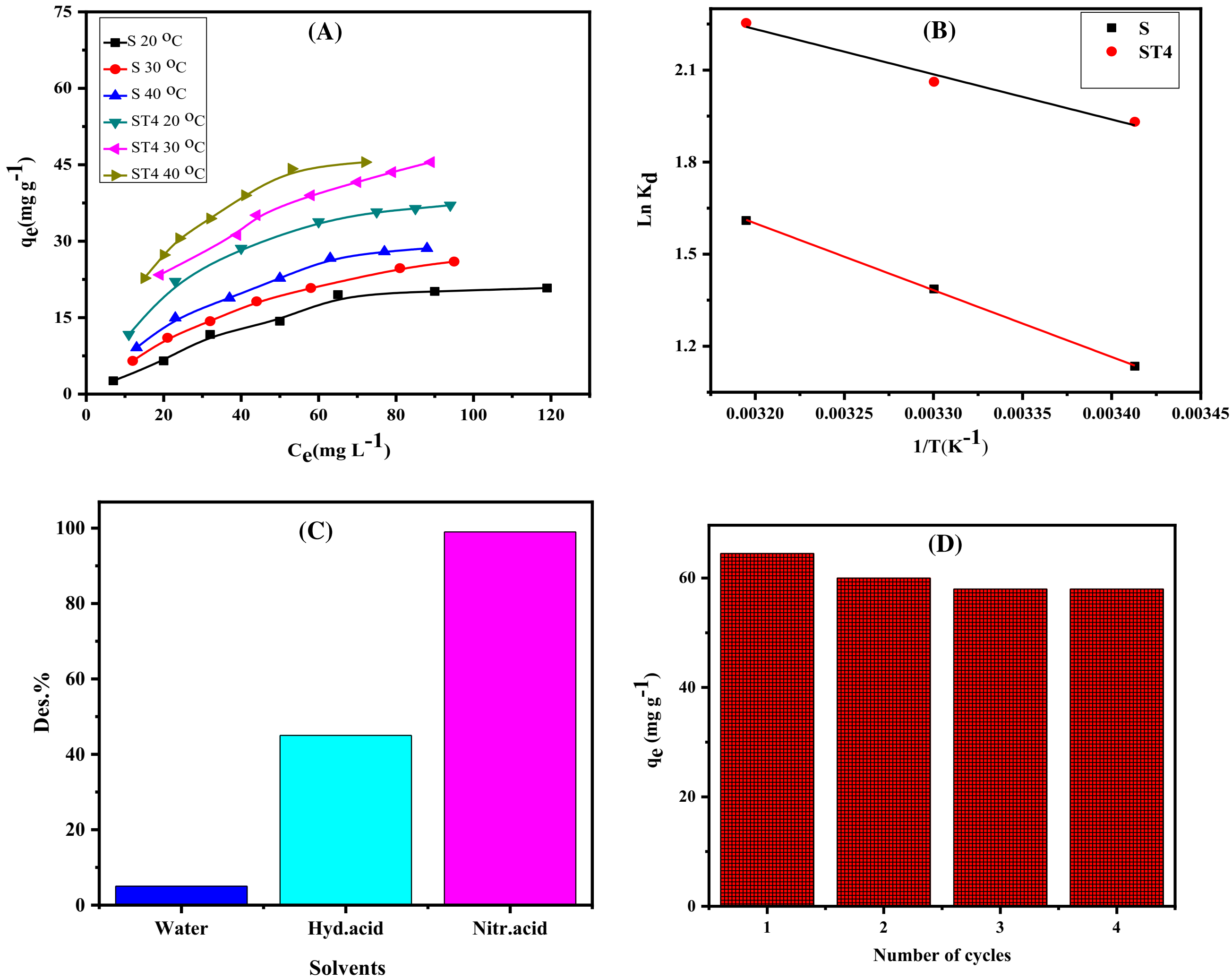

Fig. 6 Adsorption isotherms of As^{+5} onto S and ST4 at 20, 30, and 40 °C (**a**), van't Hoff plot (**b**) desorption of As^{+5} from ST4 using different solvents (**c**), and ST4 reusability after four adsorption/desorption cycles (**d**)

as shown in Fig. 6d. It is revealed that the solid adsorbent is reusable even after four cycles of adsorption where its adsorption efficiency decreased only by 9.1% and that decrease may be explained by the coagulation of nanosolid adsorbent particles, which leads to the decrease in surface area besides the expected loss of some surface chemical functional groups [50].

3.4 Comparison of ST4 with other nanosolid adsorbents

In this study, ST4 was compared with other nanosolid adsorbents as indicated in Table 4 [4, 51–56]. The reported data in the table represent the higher efficiency for trizma base-treated solid sample as a promising adsorbent for one of the most toxic heavy metal ions in the environment (As^{+5}).

Table 4 Comparison of ST4 maximum adsorption capacity with different nanosolid adsorbents

Adsorbents	q_m (mg g^{-1})	References
Chitosan–magnetic-graphene oxide (CMGO) nanocomposite	45.00	[4]
ZIF-8	60.20	[51]
Fe_3O_4-GO-MnO_2	12.22	[52]
NCuO (II)	22.60	[53]
$NTiO_2$ amorphous	19.00	[54]
Nano zero-valent@activated carbon	12.02	[55]
Fe_3O_4 nanomaterial	6.71	[56]
ST4	64.50	[The present work]

4 Conclusions

Trizma base-modified mesoporous silica nanospheres displayed high adsorption capacity to As^{+5}. Modification with trizma base enhances the adsorption efficiency of the prepared mesoporous nanosilica spheres. Static adsorption experiments revealed the good application of Langmuir, Temkin, and Dubinin–Radushkevich adsorption models with maximum adsorption capacity about 64.5 mg g^{-1}, and the optimum adsorption efficiency was achieved at pH 6, after 60 min of shaking time, and 0.9 g L^{-1} as adsorbent dosage. As^{+5} adsorption onto the prepared nanosolid materials obeyed pseudo-second-order and Elovich kinetic models. Thermodynamic parameters confirm the spontaneous, endothermic, and chemisorption adsorption process. The prepared nanosolid adsorbent showed accepted reusability after four cycles of adsorption, and the maximum desorption efficiency was confirmed by using nitric acid as a desorbing solvent. The previous experimental data considering the comparison section (Sect. 3.4) prove the promising future for trizma base-modified mesoporous nanosilica in the removal of As^{+5} from aqueous media.

Acknowledgements The authors acknowledge the research sector of Damanhour University, Damanhour, Egypt, for financial support.

Compliance with Ethical Standards

Conflict of interest The authors declare that they have no conflict of interest.

References

1. Abdel-Fattah, T.M.; Mahmoud, M.E.: Selective extraction of toxic heavy metal oxyanions and cations by a novel silica gel phase functionalized by vitamin B4. Chem. Eng. J. **172**, 177–183 (2011)
2. Vega, M.P.B.; Hinojosa-Reyes, M.; Hernández-Ramírez, A.; Guzmán Mar, J.L.; Rodríguez-González, V.; Hinojosa-Reyes, L.: Visible light photocatalytic activity of sol–gel Ni-doped TiO_2 on p-arsanilic acid degradation. J. Sol-Gel. Sci. Technol. **85**, 723–731 (2018)
3. Huang, Y.; Yang, Y.; Hu, H.; Xu, M.; Liu, H.; Li, X.; Wang, X.; Yao, H.: A deep insight into arsenic adsorption over γ-Al_2O_3 in the presence of SO_2 /NO. Proc. Combust. Inst. **37**, 2951–2957 (2019)
4. Sherlala, A.I.A.; Raman, A.A.A.; Bello, M.M.; Buthiyappan, A.: Adsorption of arsenic using chitosan magnetic graphene oxide nanocomposite. J. Environ. Manag. **246**, 547–556 (2019)
5. Li, Z.; Liu, X.; Jin, W.; Hu, Q.; Zhao, Y.: Adsorption behavior of arsenicals on MIL-101(Fe): the role of arsenic chemical structures. J. Colloid Interface Sci. **554**, 692–704 (2019)
6. Mohammed, T.; Kazeem, T.S.; Essa, M.H.; Labaran, B.A.; Vohra, M.S.: Comparative study on electrochemical treatment of arsenite: effects of process parameters, sludge characterization and kinetics. Arab. J. Sci. Eng. **45**, 3799–3815 (2020)
7. An, B.; Steinwinder, T.R.; Zhao, D.: Selective removal of arsenate from drinking water using a polymeric ligand exchanger. Water Res. **39**, 4993–5004 (2005)
8. Luo, M.K.; Lin, H.; He, Y.H.; Li, B.; Dong, Y.B.; Wang, L.: Efficient simultaneous removal of cadmium and arsenic in aqueous solution by titanium-modified ultrasonic biochar. Bioresour. Technol. **284**, 333–339 (2019)
9. Da Silva, E.B.; de Oliveira, L.M.; Wilkie, A.C.; Liu, Y.; Ma, L.Q.: Arsenic removal from As-hyperaccumulator *Pteris vittata* biomass: coupling extraction with precipitation. Chemosphere **193**, 288–294 (2018)
10. Yue, T.; Niub, Z.; Hu, Y.; Han, H.; Sun, W.; Tian, J.; Xu, Z.; Wang, L.; Yang, Y.: Arsenic adsorption on ferric oxyhydroxide gel at high alkalinity for securely recycling of arsenic-bearing copper slag. Appl. Surf. Sci. **478**, 213–222 (2019)
11. Leslie, L.A.T.; María, M.B.: Predicting the adsorption capacity of iron nanoparticles with metallic impurities (Cu, Ni and Pd) for arsenic removal: a DFT study. Adsorption **26**, 127–139 (2020)
12. Hashim, M.A.; Kundu, A.; Mukherjee, S.; Ng, Y.; Mukhopadhyay, S.; Redzwan, G.; Gupta, B.S.: Arsenic removal by adsorption on activated carbon in a rotating packed bed. J. Water Process Eng. **30**, 100591–100560 (2019)
13. Hu, C.; Chen, Q.; Li, H.; Qu, J.: Coagulation of methylated arsenic from drinking water: influence of methyl substitution. J. Hazard. Mater. **293**, 97–104 (2015)
14. Zhang, A.; Huang, N.; Zhang, C.; Zhao, P.; Lin, T.; He, Y.: Heterogeneous Fenton decontamination of organoarsenicals and simultaneous adsorption of released arsenic with reduced secondary pollution. Chem. Eng. J. **344**, 1–11 (2018)
15. Sandhi, A.; Landberg, T.; Greger, M.: Phytofiltration of arsenic by aquatic moss (*Warnstorfia fluitans*). Environ. Pollut. **237**, 1098–1105 (2018)
16. Alakhras, F.; Ouerfelli, N.; Al-Mazaideh, G.; Ababneh, T.; Al-Abbad, E.; Abouzeid, F.: Optimal pseudo-average order kinetic model for correlating the removal of nickel ions by adsorption on nanobentonite. Arab. J. Sci. Eng. **44**, 159–168 (2019)
17. Duran, H.; Alkan, F.Ü.; Ulkay, M.B.; Karakuş, S.; Aktş, A.; Şişmanoğlu, T.: Investigation of the in vitro cytotoxic effects and wound healing activity of ternary composite substance (hollow silica sphere/gum arabic/methylene blue). Int. J. Biol. Macromol. **121**, 1194–1202 (2019)
18. Ruffel, L.; Soulié, J.; Coppel, Y.; Roblin, P.; Brouillet, F.; Tourbin, M.: Ibuprofen loading into mesoporous silica nanoparticles using Co-Spray drying: a multi-scale study. Microporous Mesoporous Mater. **291**, 109689–109699 (2020)
19. Wang, X.; Zhao, Z.: Spherical hollow mesoporous silica supported phosphotungstic acid as a promising catalyst for α-arylstyrenes synthesis via Friedel-Crafts alkenylation. Chin. Chem. Lett. **30**(3), 729–734 (2019)
20. Shuangqing, S.; Xiyu, Z.; Meng, C.; Yan, W.; Chunling, L.; Songqing, H.: Facile preparation of redox-responsive hollow mesoporous silica spheres for the encapsulation and controlled release of corrosion inhibitors. Prog. Org. Coat. **136**, 105302–105310 (2019)
21. Zong, J.; Zhang, Y.S.; Zhu, Y.; Zhao, Y.; Zhang, W.; Zhu, Z.: Rapid and highly selective detection of formaldehyde in food using quartz crystal microbalance sensors based on biomimetic poly-dopamine functionalized hollow mesoporous silica spheres. Sens. Actuators B. Chem. **271**, 311–320 (2018)
22. Kalhor, M.M.; Rafati, A.A.; Rafati, L.: Synthesis, characterization and adsorption studies of amino functionalized silica nano hollow sphere as an efficient adsorbent for removal of imidacloprid pesticide. J. Mol. Liq. **266**, 453–459 (2019)
23. Najafi, M.; Yousefi, Y.; Rafati, A.A.: Synthesis, characterization and adsorption studies of several heavy metal ions on

amino-functionalized silica nano hollow sphere and silica gel. Sep. Purif. Technol. **85**, 193–205 (2012)
24. Hassan, A.F.: Synthesis of carbon nano-onion embedded metal–organic frameworks as an efficient adsorbent for cadmium ions: kinetic and thermodynamic studies. Environ. Sci. Pollut. Res. **26**(23), 24099–24111 (2019)
25. Langmuir, I.: The adsorption of gases on plane surfaces of glass, mica and platinum. J. A. Chem. Soc. **38**, 2221–2295 (1916)
26. Hyun-Kyu, L.; Jung-Weon, C.; Sang-June, C.: Magnetic ion-imprinted polymer based on mesoporous silica for selective removal of Co (II) from radioactive wastewater. Sep. Sci. Technol. (2020). https://doi.org/10.1080/01496395.2020.1797798
27. Dada, A.O.; Olalekan, A.P.; Olatunya, A.M.: Langmuir, Freundlich, Temkin and Dubinin–Radushkevich isotherms studies of equilibrium sorption of Zn^{2+} unto phosphoric acid modified rice husk. J. Appl. Chem. **3**(1), 38–45 (2012)
28. Banerjee, S.; Chattopadhyaya, M.C.: Adsorption characteristics for the removal of a toxic dye, tartrazine from aqueous solutions by a low-cost agricultural by-product. Arab. J. Chem. **10**, S1629–S1638 (2017)
29. Hassan, A.F.; Elhadidy, H.: Production of activated carbons from waste carpets and its application in methylene blue adsorption: Kinetic and thermodynamic studies. J. Environ Chem. Eng. **5**, 955–963 (2017)
30. Yuan, J.; Zhou, T.; Pu, H.: Nano-sized silica hollow spheres: Preparation, mechanism analysis and its water retention property. J. Phys. Chem. Solids. **71**, 1013–1019 (2010)
31. Chitra, K.; Annadurai, G.: Fluorescent silica nanoparticles in the detection and control of the growth of pathogen. J. Nanotechnol. **7**(17), 1–7 (2013)
32. Shitre, P.V.; Harale, R.R.; Sathe, B.R.; Shingare, M.M.S.: Silica nanosphere-graphene oxide (SiO_2–GO) hybrid catalyzed facile synthesis of functionalized quinoxaline derivatives. Res. Chem. Intermed. **43**, 829–841 (2017)
33. Gorji, B.; Ghasri, M.R.A.; Fazaeli, R.; Niksirat, N.: Synthesis and characterizations of silica nanoparticles by a new sol-gel method. J. Appl. Chem. Res. **6**(3), 22–26 (2012)
34. Skwarek, E.; Goncharuk, O.; Sternik, D.; Janusz, W.; Gdula, K.; Gun'ko, V.M.: Synthesis, structural, and adsorption properties and thermal stability of nanohydroxyapatite/polysaccharide composites. Nanoscale Res. Lett. **12**, 155–166 (2017)
35. Hassan, A.F.; Helmy, S.A.; Donia, A.: MCM-41 for meloxicam dissolution improvement: in vitro release and in vivo bioavailability studies. J. Brazil. Chem. Soc. **26**(7), 1367–1378 (2015)
36. Zhang, Y.; Cao, X.; Sun, J.; Wu, G.; Wang, J.; Zhang, D.: Synthesis of pyridyl Schiff base functionalized SBA-15 mesoporous silica for the removal of Cu (II) and Pb (II) from aqueous solution. J. Solgel Sci. Technol. **94**, 658–670 (2019)
37. Romero, A.A.; Alba, M.D.; Zhou, W.; Klinowski, J.: Synthesis and characterization of the mesoporous silicate molecular sieve MCM-48. J. Phys. Chem. **101**, 5294–5300 (1997)
38. White, L.D.; Tripp, C.P.: Reaction of (3-Aminopropyl) dimethylethoxysilane with amine catalysts on silica surfaces. J. Colloid Interface Sci. **232**, 400–407 (2000)
39. Chen, B.; Quan, G.; Wang, Z.; Chen, J.; Wu, L.; Xu, Y.; Li, G.; Wu, C.: Hollow mesoporous silica as a drug solution delivery system for insoluble drugs. Powder Technol. **240**, 48–53 (2013)
40. Mahmoud, M.E.; Fekry, N.; El-Latif, M.M.A.: Nanocomposites of nanosilica-immobilized-nanopolyaniline and crosslinked nanopolyaniline for removal of heavy metals. Chem. Eng. J. **304**, 679–691 (2016)
41. Su, H.; Ye, Z.; Hmidi, N.: High-performance iron oxide-graphene oxide nanocomposite adsorbents for arsenic removal. Colloids Surf. A Physicochem. Eng. Asp. **522**, 161–172 (2017)
42. Escudero, C.; Fiol, N.; Villaescusa, I.; Bollinger, J.C.: Arsenic removal by a waste metal (hydr) oxide entrapped into calcium alginate beads. J. Hazard. Mater. **164**, 533–541 (2009)
43. Wu, F.; Tseng, R.; Juang, R.: Characteristics of Elovich equation used for the analysis of adsorption kinetics in dye-chitosan systems. Chem. Eng. J. **150**, 366–373 (2009)
44. Zhang, Y.; Jin, F.; Shen, Z.; Lynch, R.; Al-Tabbaa, A.: Kinetic and equilibrium modeling of MTBE (methyl tert-butyl ether) adsorption on ZSM-5 zeolite: batch and column studies. J. Hazard. Mater. **347**, 461–469 (2018)
45. Erhayem, M.; Al-Tohami, F.; Mohamed, R.; Ahmida, K.: Isotherm, kinetic and thermodynamic studies for the sorption of mercury (II) onto activated carbon from rosmarinus officinalis leaves. Am. J. Anal. Chem. **6**, 1–10 (2015)
46. Shahmohammadi, K.S.H.; Babazadeh, H.; Nazemi, A.H.; Manshouri, M.: Isotherm and kinetic studies on adsorption of Pb, Zn and Cu by Kaolinite. Casp. J. Environ. Sci. **9**, 243–255 (2011)
47. Helfferich, F.: Ion Exchange. McGraw-Hill, New York (1962)
48. Bertolini, T.C.R.; Izidoro, J.C.; Magdalena, C.P.; Fungaro, D.A.: Adsorption of crystal violet dye from aqueous solution onto zeolites from coal fly and bottom ashes. Electron. J. Chem. **5**(3), 179–191 (2013)
49. Agarwal, S.; Tyagi, I.T.; Gupta, V.K.; Ghasemi, N.; Shahivand, M.; Ghasemi, M.: Kinetics, equilibrium studies and thermodynamics of methylene blue adsorption on Ephedra strobilacea saw dust and modified using phosphoric acid and zinc chloride. J. Mol. Liq. **218**, 208–218 (2016)
50. Bulánek, R.; Hrdina, R.; Hassan, A.F.: Preparation of polyvinylpyrrolidone modified nanomagnetite for degradation of nicotine by heterogeneous Fenton process. J. Environ. Chem. Eng. **7**, 102988–102997 (2019)
51. Jian, M.; Liu, B.; Hang, Z.G.; Liu, R.; Zhang, X.: Adsorptive removal of arsenic from aqueous solution by zeolitic imidazolate framework-8 (ZIF-8) nanoparticles. Coll. Surf. A. **465**, 67–76 (2015)
52. Malana, M.A.; Qureshi, R.B.; Ashiq, M.N.: Adsorption studies of arsenic on nano aluminum doped manganese copper ferrite polymer (MA, VA, AA) composite: kinetics and mechanism. Chem. Eng. J. **172**, 721–727 (2011)
53. Martinson, C.; Reddy, K.: Adsorption of arsenic (III) and arsenic (V) by cupric oxide nanoparticles. J. Colloid Interface Sci. **336**, 406–441 (2009)
54. Habuda-Stanić, M.; Nujić, M.: Arsenic removal by nanoparticles: a review. Environ. Sci. Pollut. Res. **22**, 8094–8123 (2015)
55. Zhu, H.; Jia, Y.; Wu, X.; Wang, H.: Removal of arsenic from water by supported nano zero-valent iron on activated carbon. J. Hazard. Mater. **172**(2–3), 1591–1596 (2009)
56. Luther, S.; Borgfeld, N.; Kim, J.; Parsons, J.G.: Removal of arsenic from aqueous solution: a study of the effects of pH and interfering ions using iron oxide nanomaterials. Microchem. J. **101**, 30–36 (2012)